Vol. 627: 13–31, 2019
https://doi.org/10.3354/meps13083

MARINE ECOLOGY PROGRESS SERIES
Mar Ecol Prog Ser

Published September 26

Uncertainties in variable fluorescence and ^{14}C methods to estimate primary production: a case study in the coastal waters off the Korean peninsula

Eunho Ko[1,2], Jisoo Park[1,2], Maxim Y. Gorbunov[3], Sinjae Yoo[2,4,*]

[1]Division of Polar Ocean Environment, Korea Polar Research Institute, 26 Songdomirae-ro, Yeonsu-Gu, Incheon 21990, Republic of Korea

[2]University of Science and Technology, 217 Gajeongh-ro, Daejeon 34113, Republic of Korea

[3]Department of Marine and Coastal Sciences, Rutgers University, New Brunswick, New Jersey 08901, USA

[4]Jeju Marine Research Section, Korea Institute of Ocean Science & Technology, 2670 lljudong-ro, Gujwa-eup, Jeju-si, Jeju-do 63349, Republic of Korea

ABSTRACT: To understand what controls the decoupling of photosynthetic electron transfer and carbon fixation in natural phytoplankton communities, we compared the primary production rates estimated by ^{14}C uptake and fast repetition rate fluorometry (FRRF) in Korean waters under diverse environmental conditions. Our comparison showed that these 2 methods produce consistent results, with the FRRF method systematically yielding 1.9 times higher values than the ^{14}C method. To quantify the potential factors that contribute to this discrepancy, we analyzed the variability in the electron requirement for carbon fixation, which showed a wide range of 5.5–71.3 mol electrons (mol CO_2)$^{-1}$, in relation to environmental variables. The analysis revealed that nutrient availability and the state of stratification may be the major factors that control variability in the electron requirement for carbon fixation. The strong dependence on nitrogen suggests that photosynthetic processes and phytoplankton growth are not in balance in natural communities. Based on the relationship with environmental variables, we propose a regional algorithm for the electron requirement for carbon fixation, which markedly improves FRRF-based measurements of primary production in this geographical area.

KEY WORDS: Primary production · ^{14}C · Variable fluorescence · Electron requirement for carbon fixation · Electron transfer rate · Fast repetition rate fluorometry

1. INTRODUCTION

Phytoplankton perform photosynthesis to convert inorganic carbon to organic matter using the energy of light. Primary production is defined as the synthesis of biomass through the process of photosynthesis. Quantification of primary production is critical for understanding the carbon cycle and the energy conversion processes in marine ecosystems. While phytoplankton biomass in the ocean is only about 1–2% of that of terrestrial plants, phytoplankton contribute about half of the global primary production on Earth (Falkowski 1994, Field et al. 1998, Behrenfeld et al. 2001).

Several methods are available to estimate aquatic primary production. Presumably, the oldest technique is the light and dark bottle method that measures the production of oxygen during photosynthesis; the advantage of this method is that the net primary production can be determined. Another technique measures photosynthetic carbon assimilation using radioactive or stable isotopes such as ^{14}C and ^{13}C; the

*Corresponding author: sjyoo@kiost.ac.kr

Publisher: Inter-Research · www.int-res.com

advantage of the radiocarbon method is its extreme sensitivity. Disadvantages of both methods are related to bottle effects such as heterotrophic respiration, zooplankton grazing, and effects of toxic agents (Jackson 1983, Gallegos & Platt 1985, Cullen et al. 1992). More recently, various methods that use active fluorescence have been developed and used to measure gross primary production (Kolber & Falkowski 1993). The main principle of these methods is to follow the change in the quantum yield of chlorophyll fluorescence and to derive photosynthetic parameters related to the activities of photosystem II (PSII; Kolber et al. 1998). Pulse amplitude modulation and fast repetition rate fluorometry (FRRF) are among the commonly used fluorometric methods to estimate photosynthetic parameters and gross primary production in lakes and oceans (Suggett et al. 2001, 2006, 2010, Melrose et al. 2006, Morelle et al. 2018). Fluorometric methods for determining primary production are non-intrusive, instantaneous, and sensitive, and they can measure the fluorescence variables in real time (Kolber et al. 1998). FRRF is suitable for use directly in the open ocean because of its high sensitivity (Babin et al. 1996, Aiken et al. 2000).

Despite the many advantages, there are still certain issues of accuracy and comparability of fluorometric methods, which arise from the complexity of the physiological processes involved. Fluorometric methods require assumptions on some parameters which are not directly measurable, and this inevitably introduces errors. Comparability with traditional methods is also important because our understanding of primary production in the world ocean is historically based on traditional radiocarbon measurements (Longhurst et al. 1995). To this end, studies have been carried out in several biogeochemically distinctive regions of the world ocean to compare FRRF-derived and ^{14}C-based rates of primary production. These studies found a significant relationship between these 2 techniques, but typically the FRRF-derived primary production was higher than the ^{14}C-based primary production (Moore et al. 2003, Estevez-Blanco et al. 2006, Cheah et al. 2011).

Detailed laboratory studies of phytoplankton growth in controlled chemostat experiments suggest that under balanced steady-state growth, the electron requirements for carbon fixation are virtually independent of the extent of nitrogen limitation (Halsey et al. 2010, 2011). This result appears to be in striking contrast to the field measurements that showed marked variations in the electron requirements for carbon fixation in the ocean (Lawrenz et al. 2013). In this paper, we focused on resolving this apparent paradox and on better understanding the factors that control electron requirements for carbon fixation *in situ*.

Here, we present and analyze an extensive dataset of parallel FRRF and ^{14}C-derived estimates of primary production conducted in the coastal waters off the Korean peninsula, including the Yellow Sea, East Sea, and Yeosu Bay (southern coastal area) in 2000–2012. These represent a wide range of environmental conditions and phytoplankton community structure. Our results corroborate previous field observations and clearly suggest that N limitation has a significant impact on the electron requirements for carbon fixation in natural phytoplankton communities. This implies that photosynthetic processes and phytoplankton growth in the ocean are not balanced.

2. MATERIALS AND METHODS

2.1. Sampling

Sampling and field measurements were carried out in Korean waters from May 2000 to November 2012 (Fig. 1). We conducted 8 cruises with a total of 40 stations. Sampling regions were located in the coastal waters in the East Sea (ES), Yellow Sea (YS), and Yeosu Bay (YB). In the ES and YS, measurements were taken on consecutive days in May 2000 and August 2001, respectively. In the YB, seasonal measurements were performed 6 times (August and November 2011, and February, April, August, and November 2012). For each station, hydrographic data were collected using a conductivity-temperature-depth instrument (CTD SBE-25, Sea-Bird Electronics) equipped with a transmissometer and a photosynthetically active radiation (PAR) sensor. Water samples were collected with 5 or 10 l Niskin bottles and were used to measure chlorophyll *a* (chl *a*) concentrations, nutrients, and ^{14}C uptake. Chl *a* samples were filtered at low pressure through a glass fiber filter (Whatman GF/F), then extracted in the dark for 24 h with 90% acetone. Thereafter, chl *a* concentrations were measured using a Turner Designs fluorometer (TD-700). Water samples for nutrient analysis were placed in 50 ml bottles and stored in a freezer (<–20°C). After filtering through 25 mm Whatman GF/Fs for nutrient analysis, the filtrate was measured by an automatic analyzer (Proxima, Alliance Instruments), and these measurements were validated against a standard seawater sample (CSK standard solution, Wako Pure Chemical Industries). The vertical attenuation coefficient of PAR (K_{PAR}) was

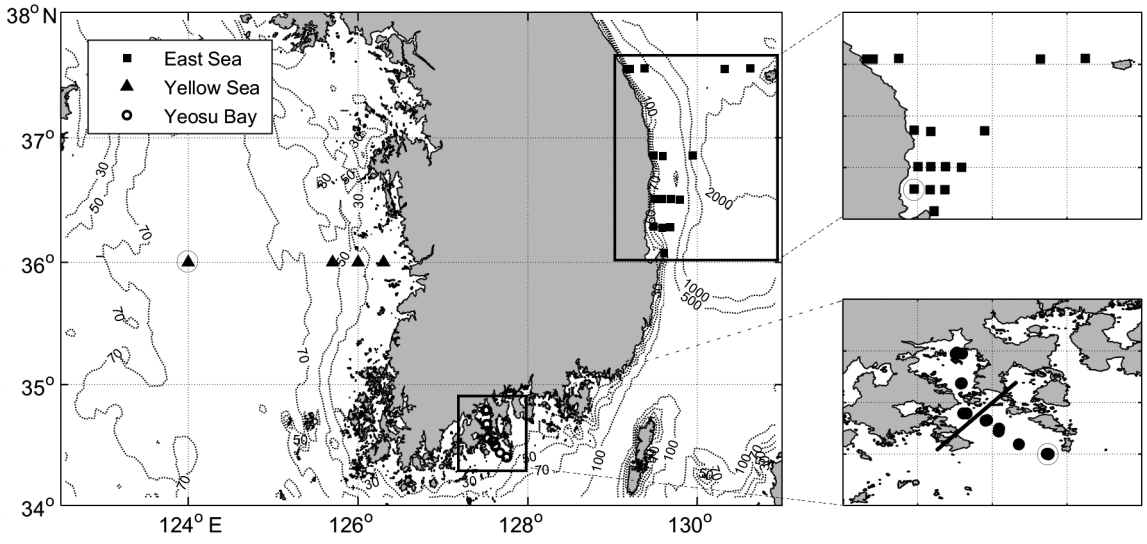

Fig. 1. Sampling stations in Korean waters. The circled markers represent the 3 stations (1 in each region) whose nutrient profiles are shown in Fig. 3. In Yeosu Bay (bottom right inset), the solid line separates the inner bay from the outer bay

estimated from the slope of the regression of the natural log-transformed PAR profile (Kirk 1977). When a PAR profile was not available, K_{PAR} was calculated from Secchi depth (K_{PAR} = 1.44/Secchi depth; Holmes 1970). We measured the daily irradiance (E_0) in the field by a quantum sensor with a logger (LI-1000, LI-COR). We also used the daily monitored E_0 data from the Korea Meteorological Administration (www.kma.go.kr/eng/index.jsp).

2.2. ^{14}C measurements

Photosynthesis-irradiance (P-E or P-I) experiments were conducted using the ^{14}C technique (details are described in Yoon et al. 2012). Water samples (n = 22) collected from 1–20 m depth were used for ^{14}C incubations. Three of these samples were from the subsurface chlorophyll maximum layer (Fig. 2). Samples were spiked with 0.025–0.05 µCi ml^{-1} of $NaH^{14}CO_3$ and incubated for 2 h at 10–12 light intensities ranging from 0 to 1500 µmol photons m^{-2} s^{-1}. Incubators equipped with a circulating water bath to maintain the *in situ* temperature were used. At the end of each incubation, samples were filtered through 0.45 µm membrane filters under low vacuum pressure (<200 mm Hg), and the filters were placed into scintillation vials. To remove inorganic carbon, the filters were fumed with 3 N HCl for 24 h under a ventilating hood. After fuming, 10 ml of scintillation cocktail was added and the samples were counted using a liquid scintillation analyzer (TRI-CARB 2910 TR, Perkin Elmer).

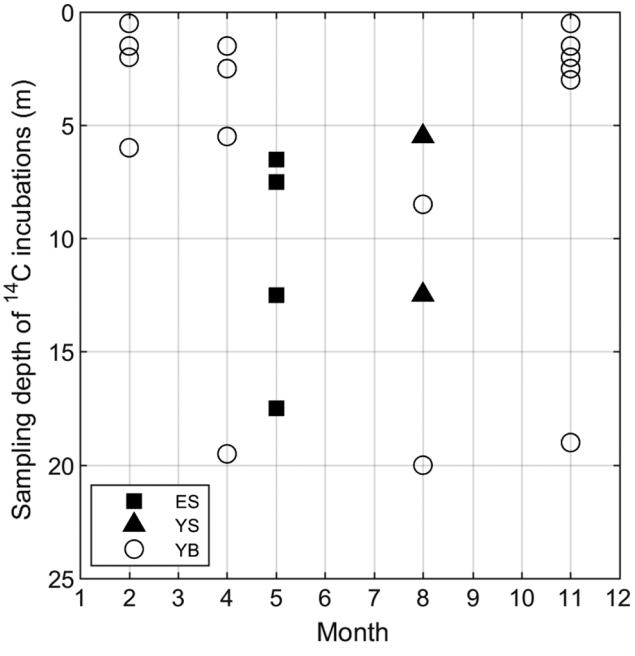

Fig. 2. Sampling depth of ^{14}C incubations by region (n = 22). Three samples from depths deeper than 15 m in April to August were from the subsurface chlorophyll maximum layer. ES: East Sea; YS: Yellow Sea; YB: Yeosu Bay

P-E parameters were then calculated using the P-E equation proposed by Platt et al. (1980):

$$P^B = P_0^B + P_m^B [1 - e^{-(\alpha^B/P_m^B)E}] \quad (1)$$

where P^B (mgC (mg chl *a*)$^{-1}$ h^{-1}) is the chl *a* normalized rate of carbon incorporation at a given light intensity; P_m^B (mgC (mg chl *a*)$^{-1}$ h^{-1}) is the assimilation number; α (mgC (mg chl *a*)$^{-1}$ h^{-1} (µmol photons

$m^{-2}\ s^{-1})^{-1}$) is the initial slope of the P-E curve; and E is the irradiance (µmol photons $m^{-2}\ s^{-1}$). Note that P_0^B (the intercept on the ordinate) was added so that the second term on the right side describes gross primary production (i.e. production becomes 0 when irradiance is 0). The ^{14}C-based primary production rate in the water column ($P_{14C}(z)$ mgC $m^{-3}\ h^{-1}$) was obtained from the P^B and chl *a* concentration at depth z:

$$P_{14C}(z) = P^B(z)\ \text{chl}\ a(z) \quad (2)$$

2.3. FRRF measurements

A Fast^{tracka} (FRRF, Chelsea Instruments) integrated with a PAR sensor was used for profiles. The unit was equipped with a light and a dark chamber and operated on the single turnover protocol that provided a flash sequence consisting of a series of 100 saturation flashes (1.1 µs flash duration and 2.8 µs inter-flash period) and a series of 20 relaxation flashes (1.1 µs flash duration and 51.6 µs inter-flash period). The gain of the FRRF detector was automatically controlled. Data from FRRF were fitted to the biophysical model (Kolber et al. 1998) using post-processing software (FRS v1.8) provided by Chelsea Instruments. The fluorescence parameters and related variables are defined in Table 1. Among these parameters, F_0' was difficult to measure accurately (see Kromkamp & Forster 2003); we therefore estimated F_0' using the equation given in Table 1 (Oxborough & Baker 1997, Suggett et al. 2003). The raw FRRF data were first screened for data quality based on the error flags and validation codes provided by the FRS software. Each profile was then also examined for fitness using the chi-squared test. After excluding the erroneous profiles, the remaining raw FRRF data were directly fitted with the fluorescence saturation curve equation proposed by Kolber & Falkowski (1993). The intercalibration of the light and dark channels was very good, as evidenced by the high correlation between F_m and F_m' (see Table 1 for definitions; slope = 0.99, $r^2 = 0.93$; data not shown).

2.4. Rationale for primary production measurements using variable fluorescence

Variable fluorescence techniques (such as FRR or fluorescence induction and relaxation [FIRe]) are used to deduce photosynthetic electron transport rates (ETRs) in PSII. Functional absorption cross-sections of PSII derived from FRR measurements allow for the ETR to be measured in absolute units, i.e. electrons per PSII reaction center (RCII) per unit time. The ETR per reaction center can then be converted to ETR per unit chl *a* (i.e. chlorophyll-specific ETR^{chl}) by multiplying ETR by the size of the PSII unit, n_{PSII} (i.e. the ratio of PSII reaction centers to the number of chl *a* molecules) (Kolber & Falkowski 1993). To further convert ETR^{chl} into the rates of CO_2 assimilation (or O_2 evolution), one must know how

Table 1. Fluorescence parameters. Definitions and derivations after Baker et al. (2001) and Kromkamp & Forster (2003). PSII: Photosystem II; RCII: PSII reaction center

Parameter	Definition	Derivation	Units
F_0, F_m	Minimum and maximum fluorescence in dark-adapted state		Arbitrary
F', F_m'	Steady state and maximum fluorescence under ambient light		Arbitrary
F_0'	Minimum fluorescence under ambient light	$F_0/[(F_v/F_m)+(F_0/F_m')]$	Arbitrary
F_v/F_m	Potential photochemical efficiency	$(F_m-F_0)/F_m$	Dimensionless
$\Delta F'/F_m'$	Photochemical efficiency under ambient light (also denoted as F_q'/F_m')	$(F_m'-F')/F_m'$	Dimensionless
σ_{PSII}	Functional absorption cross section of PSII		10^{-20} m^2 photon^{-1}
σ'_{PSII}	σ_{PSII} measured under ambient light		10^{-20} m^2 photon^{-1}
q_p	Photochemical quenching	$(F_m-F)/(F_m-F_0')$	Dimensionless
NPQ	Non-photochemical quenching	$(F_m - F_m')/F_m'$	Dimensionless
n_{PSII}	Photosynthetic unit size of PSII reaction centers		mol RCII (mol chl *a*)$^{-1}$
$1/k$	Quantum yield of electron transport through PSII per O_2 molecule evolved		mol O_2 (mol photons)$^{-1}$
PQ	Photosynthetic quotient		mol O_2 evolved (mol C fixed)$^{-1}$
$\Phi_{e,C}$	Electron requirement for carbon fixation		mol e^- (mol CO_2^{-1})

many electrons are needed to fix 1 molecule of CO_2 (or generate 1 molecule of O_2). As 4 electrons are needed to evolve 1 O_2, the electron yield of O_2 evolution in PSII ($1/k$) is assumed to be 0.25. CO_2 fixation rates are estimated by incorporating the ratio of O_2/CO_2, called the photosynthetic quotient (PQ), into the fluorescence-based model of primary production.

The ETR per active PSII reaction center is a function of irradiance and is calculated using the following equation (Gorbunov et al. 2000, 2001):

$$\mathrm{ETR} = E\,\sigma'_{\mathrm{PSII}}\,(\Delta F'/F_v') \quad (3)$$

where σ'_{PSII} is the functional absorption cross section of PSII and $\Delta F'/F_v'$ is the coefficient of photochemical quenching, which is the fraction of open reaction centers at a given level of irradiance; the prime character (') indicates measurements under ambient irradiance (E). Here, both σ'_{PSII} and $\Delta F'/F_v'$ are a function of irradiance.

When non-photochemical quenching is caused by thermal dissipation in the light-harvesting antennae, Eq. (3) can be reduced to the following (Gorbunov et al. 2000):

$$\mathrm{ETR} = E\,\sigma_{\mathrm{PSII}}\,[(\Delta F'/F_m')\,/\,(F_v/F_m)] \quad (4)$$

where $\Delta F'/F_m'$, which is also denoted as F_q'/F_m' in oceanographic literature, is the only irradiance-dependent variable. It should be noted that the use of Eq. (3) requires measurements under both ambient light and in the dark (e.g. in open and dark chambers of the FRR fluorometer). For instance, $F_v' = F_m' - F_0'$ can be only recorded after a brief (~1 s) period of darkness, which is required for all reaction centers to open and for fluorescence yield to reach the F_0' level. In contrast, Eq. (4) does not need F_0' measurements.

Chlorophyll-specific ETRs are calculated by multiplying Eq. (4) by the size of the photosynthetic unit, n_{PSII} (Kolber & Falkowski 1993):

$$\mathrm{ETR}^{\mathrm{chl}} = E\,\sigma_{\mathrm{PSII}}\,[(\Delta F'/F_m')\,/\,(F_v/F_m)]\,n_{\mathrm{PSII}} \quad (5)$$

n_{PSII} cannot be measured directly using variable fluorescence alone (Kolber & Falkowski 1993). Although n_{PSII} may range from 0.001 to 0.007 mol RCII (mol chl a)$^{-1}$, the FRR model assumes $n_{\mathrm{PSII}} = 0.002$, a typical average value for eukaryotic algae (Kolber & Falkowski 1993).

Chlorophyll-specific rates of CO_2 fixation are calculated by multiplying Eq. (5) by $(1/k)$/PQ:

$$P^{\mathrm{chl}} = E\,\sigma_{\mathrm{PSII}}\,[(\Delta F'/F_m')/(F_v/F_m)]\,n_{\mathrm{PSII}}\,(1/k)\,\mathrm{PQ}^{-1} \quad (6)$$

Here, the ratio $(1/k)\,\mathrm{PQ}^{-1}$ defines how many moles of CO_2 are fixed per 1 mole of electrons (e^{-1}).

2.5. FRRF-derived primary production rate

In situ chl *a* specific ETRs through PSII (mmol e^{-1} (mg chl a)$^{-1}$ h^{-1}) was determined by using Eq. (5) as follows (Kolber & Falkowski 1993, Suggett et al. 2001, Lawrenz et al. 2013):

$$\mathrm{ETR}(z) = 2.43 \times 10^{-2}\,E(z)\,\sigma_{\mathrm{PSII}}\,\Delta F'/F_m'\,F_m/F_v\,n_{\mathrm{PSII}} \quad (7)$$

Here, $E(z)$ is the irradiance at depth z, and 2.43×10^{-2} is a numerical factor to account for the conversion of σ_{PSII} from (Å^2 quanta^{-1}) to (m^2 (mol RCII)$^{-1}$), E(z) from (µmol photons m^{-2} s^{-1}) to (mol photons m^{-2} h^{-1}) and seconds to hours. The values of σ_{PSII} were spectrally corrected as described by Moore et al. (2006):

$$\sigma_{\mathrm{PSII},in\,situ} = \sigma_{\mathrm{PSII},\,478}\,(\Sigma_{400-700\,\mathrm{nm}}\,a^*(\lambda)\,E_{in\,situ}(\lambda) \geq_{400-700\,\mathrm{nm}} E_{\mathrm{FRR}}(\lambda)/\Sigma_{400-700\,\mathrm{nm}}\,a^*(\lambda)\,E_{\mathrm{FRR}}(\lambda)\,\Sigma_{400-700\,\mathrm{nm}}\,E_{in\,situ}(\lambda)) \quad (8)$$

where $a^*(\lambda)$ is the chlorophyll-specific absorption spectrum. $E_{\mathrm{FRR}}(\lambda)$ and $E_{in\,situ}(\lambda)$ refer to the excitation spectra of the FRRF and *in situ* irradiance field, respectively. The electron requirement for carbon fixation, $\Phi_{e,C}(z)$ (mol e^{-1} (mol CO_2)$^{-1}$) was calculated from $P^B(z)$, ^{14}C-based chl *a*-normalized rate of carbon incorporation (converted to mol C (mg chl a)$^{-1}$ h^{-1}), and ETR(z), as follows (Lawrenz et al. 2013):

$$\Phi_{e,C}(z) = \mathrm{ETR}(z)\,/\,P^B(z) \quad (9)$$

We estimated the *in situ* FRRF-derived primary production rate by expanding Eq. (6) as follows (Kolber & Falkowski 1993, Suggett et al. 2001, Lawrenz et al. 2013):

$$P_{\mathrm{FRRF}}(z) = 29.16 \times 10^{-2}\,E(z)\,1/k\,\sigma_{\mathrm{PSII}}\,\Delta F'/F_m'\,F_m/F_v\,n_{\mathrm{PSII}}\,\mathrm{chl}\,a(z)\,\mathrm{PQ}^{-1} \quad (10)$$

where 29.16×10^{-2} is a numerical factor to account for the conversion of σ_{PSII} from [Å^2 quanta^{-1}] to (m^2 (mol RCII)$^{-1}$), $E(z)$ from (µmol photons m^{-2} s^{-1}) to (mol photons m^{-2} h^{-1}), n_{PSII} from (mol PSII (mol chl a)$^{-1}$) and mol C to mgC. Here, 3 parameters, $1/k$, n_{PSII}, and PQ, cannot be obtained by fluorometry and should be predetermined. We used values for these parameters as follows: $n_{\mathrm{PSII}} = 0.002$ mol RCII (mol chl a)$^{-1}$ (Kolber & Falkowski 1993); PQ = 1.4 mol O_2 evolved (mol C fixed)$^{-1}$ (Laws 1991); and $1/k = 0.25$ mol O_2 (mol photons)$^{-1}$ (Kolber & Falkowski 1993).

2.6. Incubation experiments to assess the bottle effects

To assess the bottle effects in the ^{14}C technique, the same incubation setup of the P-E experiment

was used and photosynthetic responses were measured as changes in fluorometric parameters. We used 3 strains of phytoplankton species obtained from the Korean Marine Microalgae Culture Center (KMMCC). The species were *Skeletonema* sp. (strain number: KMMCC-1102), *Heterocapsa circularisquama* (KMMCC-580), and *Coscinodiscus oculoides* (KMMCC-831). All algae were grown in a batch culture at 15°C and illuminated with a 12:12 h light:dark cycle at light intensity of 110–120 µmol m^{-2} s^{-1}, and cultivated in f/2 medium (Guillard 1975). To conduct this experiment, we used specimens from the growth phase. The batches were incubated for 2 h at 5 light intensities that ranged from 42 to 928 µmol m^{-2} s^{-1}. During the incubation, each sample was measured by FIRe (Satlantic) to follow the changes in the potential photochemical efficiency (F_v/F_m) and functional absorption cross section (σ_{PSII}) at 0, 5, 60, and 120 min after the inception of each experiment. The samples were adapted in the dark for 5 min prior to the measurements.

2.7. Statistical analysis

Statistical analyses were done using MATLAB. The relationship between primary production derived by the 2 methods was statistically tested by linear regression analysis. In addition, to determine the probability of a potential error in non-fluorometric parameters on FRRF-based primary production, a Monte Carlo simulation was performed using a set of random numbers within the range of each parameter. Prior to generating a new regional algorithm for predicting the electron requirement of carbon fixation, significant environmental variables were chosen through a Spearman rank correlation between the log-transformed electron requirement of carbon fixation ($\Phi_{e,C}$) and environmental variables. We then generated 3 algorithms by combining the selected variables using multiple regression analysis.

3. RESULTS

3.1. Environmental conditions

The study regions are located around the Korean peninsula with various physical and chemical characteristics influenced by different factors such as freshwater runoff and hydrographic regimes (Fig. 1). Table 2 provides some basic information about the study regions. The ES has a deep basin and no significant river discharge. These waters are relatively clear with low levels of colored dissolved organic matter or suspended sediments. At the ES stations, E_0 ranged from 28.0 to 52.7 E m^{-2} d^{-1}. Sea surface temperature (SST) and salinity ranged from 12.4 to 17.6°C and 33.7 to 34.4 psu. Average K_{PAR} ranged from 0.08 to 0.15 m^{-1}. The YS is a shallow shelf region and optically belongs to Case 2 waters (Morel & Prieur 1977), but at the time of our observations (August), the water column was strongly stratified and turbidity was low (K_{PAR} = 0.10–0.29 m^{-1}). At the YS stations, the values of E_0 ranged from 15.7 to 40.2 E m^{-2} d^{-1}. SST and salinity ranged from 25.3 to 27.4°C and 30.3 to 31.7 psu. The YB is a shallow bay region somewhat influenced by river discharge loaded with a high level of nutrients and sediments. The YB stations could be divided into the inner and the outer bay (Fig. 1). While the inner bay is very shallow (<10 m) and strongly influenced by river discharge, the outer bay is relatively deep (15–45 m)

Table 2. Mean ± SD (range in parentheses) of representative variables on the surface (sea surface temperature [SST], salinity, chl *a*) or sample depths (P_m^B, P_{14C}, P_{FRRF}) for each region. ES: East Sea; YS: Yellow Sea; YB: Yeosu Bay; E_0: daily irradiance; K_{PAR}: vertical attenuation coefficient of photosynthetically active radiation; P_m^B: assimilation number; P_{14C}: ^{14}C-based primary production rate; P_{FRRF}: fast repetition rate fluorometry (FRRF)-based primary production rate; N(PP): the number of primary production experiments

Region	Date	E_0 (E m^{-2} d^{-1})	SST (°C)	Salinity	K_{PAR} (m^{-1})	Chl *a* (mg m^{-3})	P_m^B (mgC (mg chl *a*)$^{-1}$ h^{-1})	P_{14C} (mg C m^{-3} h^{-1})	P_{FRRF} (mgC m^{-3} h^{-1})	N	N (PP)
ES	May 2000	46.3 ± 7.9 (28.0–52.7)	15.8 ± 1.51 (12.4–17.6)	34.0 ± 0.24 (33.7–34.4)	0.12 ± 0.02 (0.08–0.15)	0.2 ± 0.1 (0.1–0.4)	2.2 ± 0.7 (1.4–2.9)	0.90 ± 0.30 (0.60–1.2)	3.6 ± 1.4 (2.1–5.4)	16	4
YS	Aug 2001	34.1 ± 12.2 (15.7–40.2)	26.3 ± 0.99 (25.3–27.4)	31.0 ± 0.59 (30.3–31.7)	0.19 ± 0.08 (0.10–0.29)	2.2 ± 1.7 (0.2–3.7)	1.8 ± 1.0 (1.1–2.5)	1.5 ± 1.7 (0.20–2.7)	2.7 ± 0.4 (2.5–2.8)	4	2
YB	Feb–Nov 2011–2012	27.9 ± 13.2 (10.4–60.5)	16.2 ± 7.36 (3.2–29.2)	31.9 ± 1.87 (28.4–34.4)	0.89 ± 0.80 (0.12–3.33)	3.3 ± 2.3 (0.2–8.0)	3.3 ± 1.7 (1.4–8.5)	3.6 ± 4.3 (0.10–13.0)	7.5 ± 8.1 (0.4–29.0)	20	16

and influenced by the Tsushima Warm Current (a branch of the Kuroshio with higher temperature and salinity). As a result, the YB stations exhibited a wide range of environmental characteristics. In the inner bay, SST and salinity ranged from 3.2°C (February) to 29.2°C (August) and from 28.4 psu (August) to 34.3 psu (February). In the outer bay, however, SST and salinity ranged from 11.8°C (February) to 26.5°C (August) and from 31.9 psu (August) to 34.4 psu (February). At the YB stations, E_0 ranged from 10.4 (February) to 60.5 $E\ m^{-2}\ d^{-1}$ (April). K_{PAR} ranged from 0.12 to 3.33 m^{-1}, which represents a wide range of turbidity from rather clear water in the outer stations to very turbid inner bay water.

3.2. Nutrient conditions

The surface concentrations of nutrients differed markedly among the regions. At the YB stations, nitrate + nitrite was higher than in other regions and ranged from 0.31 to 14.21 µmol l^{-1}, with an average value of 5.33 µmol l^{-1}. At the YS stations, the concentrations of phosphate and silicate were higher than in the other regions (0.02–2.34 µmol l^{-1} and 20.90–46.33 µmol l^{-1}, respectively), but nitrate + nitrite was lower than in other regions (1.35–2.41 µmol l^{-1}). The average concentration of phosphate (0.20 µmol l^{-1}) was lowest at the ES stations, and nitrate + nitrite ranged from 1.05 to 8.70 µmol l^{-1}. Fig. 3 shows representative profiles of nutrient concentrations in each region. At all 4 stations shown in Fig. 3, nitrate + nitrite was virtually depleted at the surface and increased below the upper mixed layer (Fig. 3a). The phosphate concentrations showed a similar trend to that of nitrate + nitrite (Fig. 3b). In the outer bay of the YB region (August), nitrate + nitrite (<1 µmol l^{-1}) and phosphate (<0.1 µmol l^{-1}) were very low at the surface.

3.3. Distribution of chl *a* and assimilation numbers

The surface chl *a* concentrations were relatively low in the ES region, ranging from 0.1 to 0.4 mg m^{-3} in May 2000 (Table 2), and a subsurface chl *a* maximum (SCM) was clearly seen at the ES stations (Fig. 3c). At the YS stations, the surface chl *a* concentrations ranged from 0.2 to 3.7 mg m^{-3} in August 2001. The highest chl *a* concentration was measured at a near-shore station in the YS; this was the only station at which the highest chl *a* concentration was

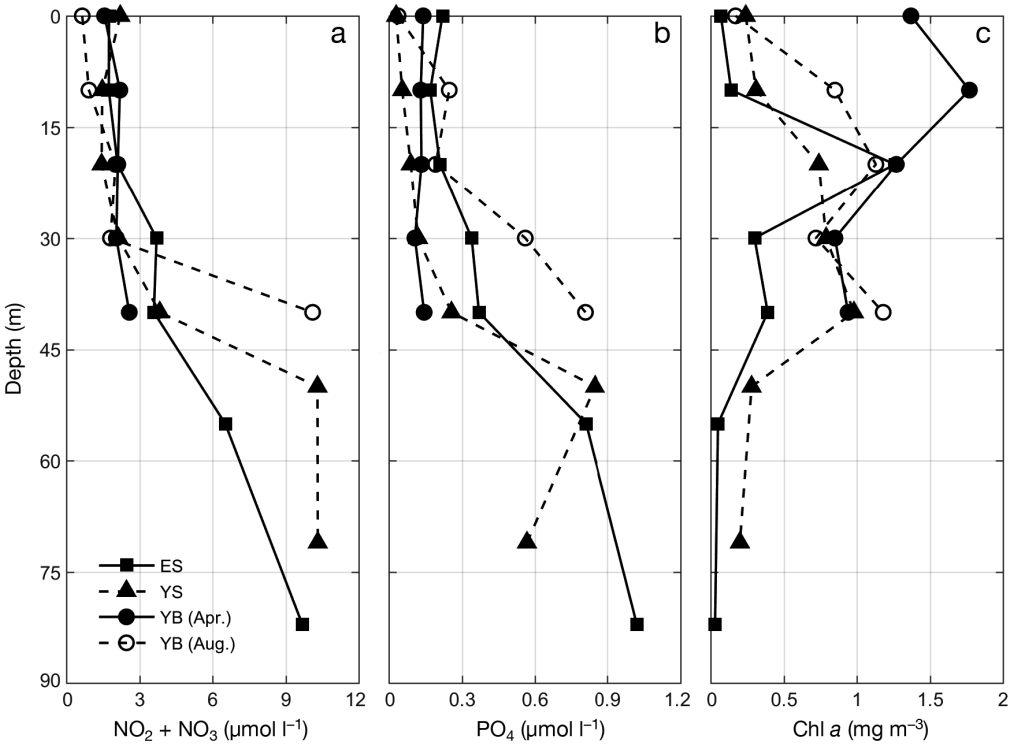

Fig. 3. Vertical profiles of nitrate + nitrite, phosphate and chlorophyll *a* by region. See Fig. 1 for the locations of the stations. ES: East Sea; YS: Yellow Sea; YB: outer Yeosu Bay

measured at the surface (Fig. 3c). At the YB stations, the surface chl *a* concentrations were higher in the inner bay (1.4–8.0 mg m^{-3}) than in the outer bay (0.2–3.6 mg m^{-3}). While the SCM was developed in the outer bay, vertical distributions of chl *a* concentrations were homogeneous in the inner bay.

P_m^B, a key parameter to calculate ^{14}C-based primary production rate, ranged from 1.4 to 2.9 mg C (chl *a*)$^{-1}$ h^{-1} in the ES. P_m^B values ranged from 1.1 to 2.5 mg C (chl *a*)$^{-1}$ h^{-1} in the YS and from 1.4 to 13.2 mg C (chl *a*)$^{-1}$ h^{-1} in the YB. P_m^B showed a similar value in the ES and the YS regions. The maximum value of P_m^B (13.2 mg C (chl *a*)$^{-1}$ h^{-1}) was obtained in the YB region.

3.4. Fluorescence variables

The fluorescence variables showed a close relationship with light levels and nutrients (Cheah et al. 2011). FRRF-derived potential photochemical efficiency (F_v/F_m) and photochemical efficiency ($\Delta F'/F_m'$) are thought to indicate the photochemical efficiency of PSII and phytoplankton physiological condition (Kromkamp & Forster 2003). F_v/F_m and $\Delta F'/F_m'$ in the study regions ranged from 0.32–0.64 and 0.15–0.60, respectively. The lowest values of these variables were measured at the surface. The divergence between F_v/F_m and $\Delta F'/F_m'$ was greater at the surface (Fig. 4). The difference between F_v/F_m

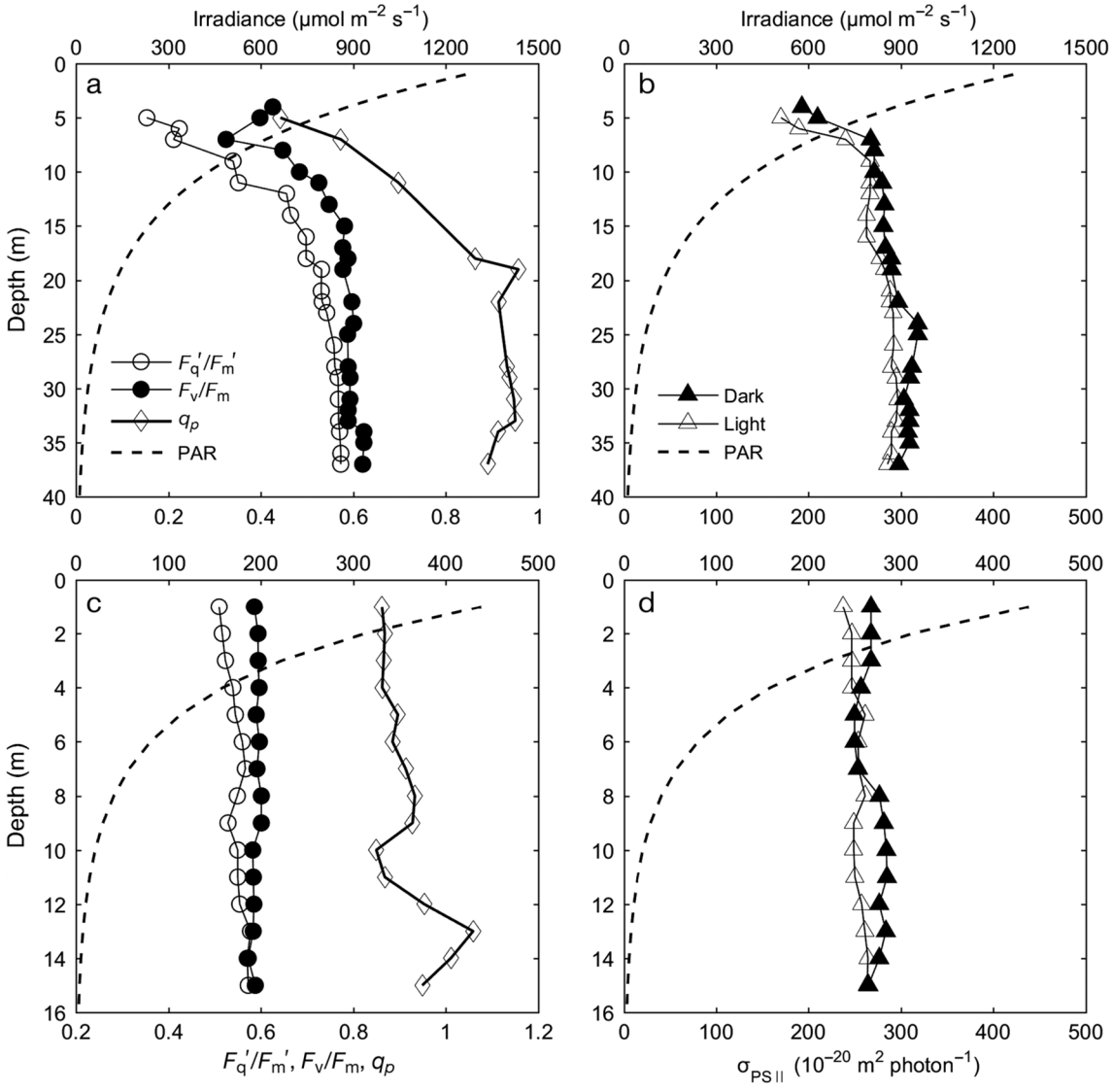

Fig. 4. Vertical profiles of F_q'/F_m', F_v/F_m, q_p, σ_{PSII} (all fluorescence parameters are defined in Table 1) and photosynthetically active radiation (PAR) at 2 stations in Yeosu Bay (YB). (a,b) Data from the outer bay of YB (April); (c,d) data from the inner bay of YB (November)

and $\Delta F'/F_m'$ at the surface can be explained by dark adaptation that gave rise to re-oxidation of *Q*a (the primary electron acceptor quinone) in the reaction centers during a very short time (Kolber & Falkowski 1993). However, these variables gradually increased with depth and nearly reached the typical maximum for phytoplankton species, 0.65 (Kolber & Falkowski 1993). The functional absorption cross section (σ'_{PSII}) is equal to the product of the optical cross section and the trapping efficiency (Kromkamp & Forster 2003). σ'_{PSII} ranged from 158 $\times 10^{-20}$ to 1324 $\times 10^{-20}$ m^2 photon^{-1}. At some stations in the ES, σ'_{PSII} decreased below the SCM (not shown). Fig. 4 shows the vertical profiles of *in situ* FRRF-derived variables in the YB. Note that the surface irradiance in Fig. 4a,b (April) is 3 times higher than that of Fig. 4c,d (November). These profiles have 2 different trends. In the outer bay, photochemical variables were low at the surface, and gradually increased with depth (Fig. 4a,b), whereas in the inner bay, the variables were constant (Fig. 4c,d). Photochemical quenching (q_p) ranged from 0.37 to 1.08. Values >1.0 contain errors associated with estimating F_0' (see Section 2.3). The vertical trend of q_p was similar to F_v/F_m and $\Delta F'/F_m'$.

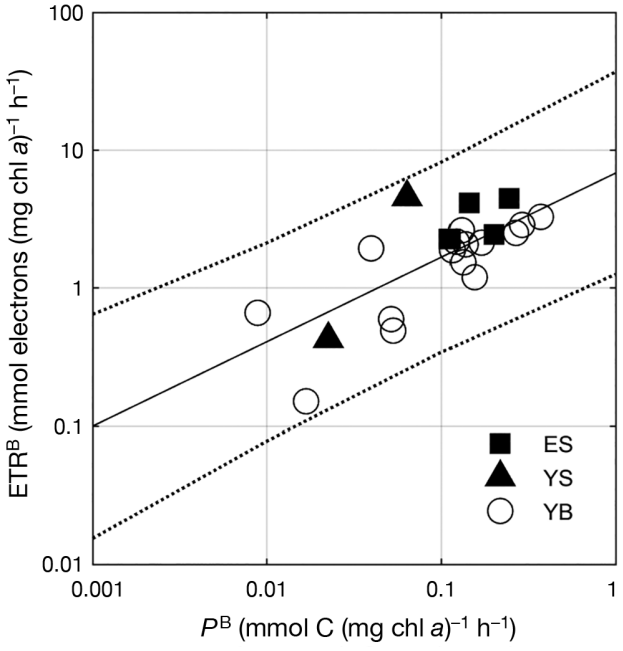

Fig. 5. Relationship between ^{14}C primary production rate (P^B: chl *a* normalized rate of carbon incorporation at a given light intensity) and electron transfer rate (ETR) normalized to chlorophyll *a* ($r^2 = 0.72$, SSE [error sum of squares] = 1.30, RMSE [root mean square error] = 0.25, $p < 0.001$, n = 22). The solid line is the regression line, and the dashed lines show the 95% confidence interval

3.5. Electron requirement for carbon fixation

Fig. 5 shows the relationship between chl *a* specific ^{14}C primary production rate (mmol C (mg chl *a*)$^{-1}$ h^{-1}) and FRRF-derived ETR(*z*) (mmol e$^-$ (mg chl *a*)$^{-1}$ h^{-1}). The statistically significant relationship ($r^2 = 0.72$, $p < 0.001$, n = 22) between these 2 values suggests that the electron requirement for carbon fixation ($\Phi_{e,C}$ (*z*)) can be estimated from the 2 values (Fig. 6). Table 3 shows the average $\Phi_{e,C}$ (*z*) in each region. The $\Phi_{e,C}$ (*z*) values for August in the YS and YB regions were higher than those in other regions, and the maximum value was recorded in the YS region. Generally, values in spring were low (Fig. 6a). Fig. 6b shows $\Phi_{e,C}$ (*z*) in the inner and the outer bay of the YB. Except for August, the trends of $\Phi_{e,C}$ (*z*) were similar in both areas; in August, this value was 10 times higher in the outer bay than in the inner bay. $\Phi_{e,C}$ (*z*) showed

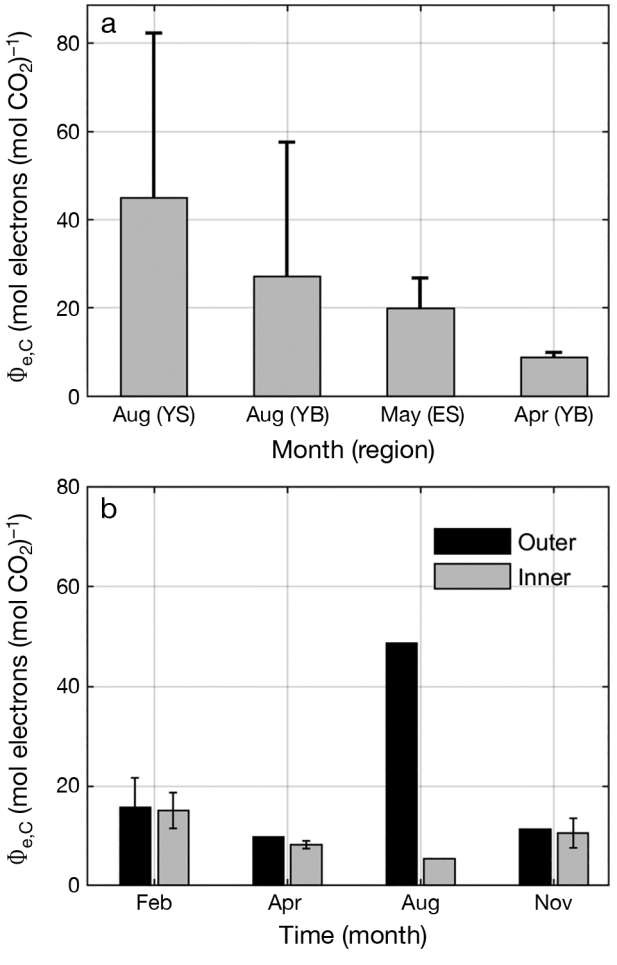

Fig. 6. Electron requirement for carbon fixation, $\Phi_{e,C}$ (mol e$^-$ (mol CO_2)$^{-1}$) compared by (a) region (ES: East Sea; YS: Yellow Sea; YB: Yeosu Bay) and (b) season in the inner and the outer bay of the YB. Error bars show the standard deviation

Table 3. Mean ± SD (range in parentheses) of the electron requirement for carbon fixation ($\Phi_{e,C}$, mol e^- mol CO_2^{-1}) at the surface by region (ES: East Sea; YS: Yellow Sea; YB: Yeosu Bay)

Region	$\Phi_{e,C}$	N
ES	19.9 ± 6.8 (12.2–28.6)	4
YS	45.1 ± 37.1 (18.8–71.3)	2
YB		
Inner	10.5 ± 3.8 (5.5–17.6)	9
Outer	20.3 ± 16.3 (9.8–48.6)	5

the minimum value in August in the inner bay, which is influenced by river discharges during the rainy season in summer.

3.6. Relationship between FRRF- and ^{14}C-based primary production rates

Primary production rates ranged from 0.6–76 and from 0.10–51 mg C m^{-3} h^{-1}, respectively, using FRRF and ^{14}C measurements (Table 2). Average FRRF-derived primary production rates were higher than ^{14}C-based primary production rates in all regions, but the degree of discrepancy between FRRF-derived and ^{14}C-based primary production estimates differed for each region. A significant linear relationship was found between FRRF- and ^{14}C-based primary production rates (r^2 = 0.90, slope = 1.94, $p < 0.001$, n = 22; Fig. 7). In particular, Fig. 7b shows that the correlation was higher at the YB stations (r^2 = 0.91, slope = 1.92, $p < 0.001$, n = 16) than at all other stations (Fig. 7a). Although there was a significant correlation between the primary production rates measured by the 2 methods, FRRF-derived primary production rates were systematically higher at all stations.

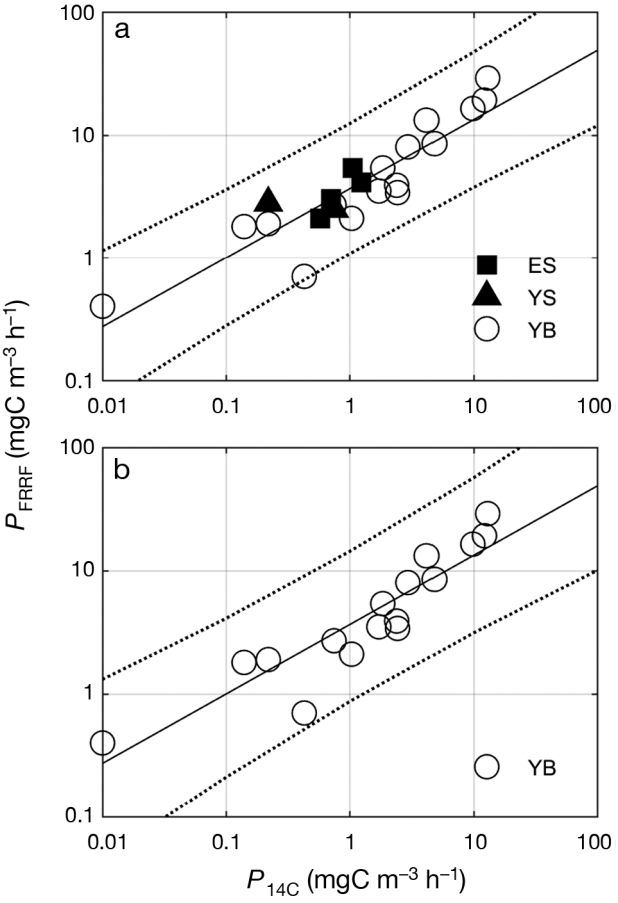

Fig. 7. Relationship between the primary production rates measured by fast repetition rate fluorometry (FRRF) and ^{14}C incubations at (a) all stations ($y = 0.56 + 0.56x$, r^2 = 0.90, $p < 0.001$, n = 22) (ES: East Sea; YS: Yellow Sea; YB: Yeosu Bay) and (b) stations in YB only ($y = 0.55 + 0.57x$, r^2 = 0.91, $p < 0.001$, n = 16). The solid line is the regression line and the dotted lines show the 95% confidence interval

4. DISCUSSION

4.1. Discrepancies between FRRF- and ^{14}C-based primary production rates

The ratio of FRRF-derived to ^{14}C-based primary productions rates was >1 for our data set. However, the significant correlation between the 2 methods indicates that they both produce consistent results. This result also confirms that the FRRF technique can be a reliable tool to calculate primary production rate (Melrose et al. 2006). In our study, the FRRF-derived primary production rates were on average 1.94 times higher than ^{14}C-based rates. This is comparable to the results of previous studies (Table 4), where the ratio of FRRF to ^{14}C-based rates ranged from 1.23 to 2.5 (Corno et al. 2006, Estevez-Blanco et al. 2006, Cheah et al. 2011). On the other hand, Moore et al. (2003) obtained FRRF-derived primary production rates that were consistently lower than ^{14}C-estimates. Those authors applied a different calculation in that the value of P_m^B was empirically extrapolated using σ_{PSII} and α^B, which were calculated from FRRF-derived variables. Other studies also showed that the FRRF-derived primary production rate was lower than the ^{14}C-based primary production rate (Smyth et al. 2004, Melrose et al. 2006). Melrose et al. (2006) argued that FRRF estimates need to be corrected because of the uncertainty of the chlorophyll fluorescence method. Kolber & Falkowski (1993) and Boyd

Table 4. Ratio (slope) of the relationship between fast repetition rate fluorometry and ^{14}C estimates from previous studies

Reference	Region	N	Ratio
Suggett et al. (2001)	North Atlantic	22	1.5–2.5
Raateoja et al. (2004)	Baltic Sea	20	0.7–1.6
Smyth et al. (2004)	Celtic Sea	6	0.8
Corno et al. (2006)	ALOHA station (North Pacific)	70	1.9–2.0
Estevez-Blanco et al. (2006)	Western Atlantic coast of Spain	16	1.43
Cheah et al. (2011)	Sub-Antarctic Zone	85	1.23
This study	Korean waters	22	1.94

et al. (1997) used another type of variable fluorescence instrument, a pump and probe fluorometer (PPF), which, although similar in principle, is significantly different/slower than the one we used here (Eqs. 5–7). Because the model of Kolber & Falkowski (1993) takes into account the fraction of active reaction centers (f) in the equation for P_{FRRF}, it results in lower P_{FRRF} rates especially in nutrient-limited waters, as compared to P_{FRRF} from the model we used (Eq. 10). Kolber & Falkowski (1993) obtained a similar relationship between PPF and radiocarbon with a slope of 1.06. Boyd et al. (1997), however, found that the primary production rate from the PPF technique was underestimated by a factor of 1.5 compared to the ^{14}C primary production rate. Therefore, it is not yet conclusive whether fluorometric methods give consistently higher or lower estimates compared to the radiocarbon method. The comparison is further complicated by inherent errors in the ^{14}C method, including incubation time and ambient light intensities, among others (Cheah et al. 2011, Milligan et al. 2015). Particularly, Halsey et al. (2010, 2011, 2013) reported that short-term ^{14}C methods are not reliable for net or gross primary production because the results of short-term incubations (<12 h) are dependent on the specific growth rate, which is associated with changes in photosynthetic storage and mobilization.

The discrepancy between FRRF-derived and ^{14}C-based primary production rates can be attributed to several possible causes. Here, we consider 4 possible sources of the discrepancy. First, there are methodological differences in the 2 techniques. When all reaction centers of PSII are open, 4 electrons (e^-) are used to generate 1 oxygen molecule. However, $e^- > 4$ is required to generate net oxygen (Flameling & Kromkamp 1998), because additional electrons are needed to produce ATP, NADPH, and reduced ferredoxin (Suggett et al. 2010). ATP is produced in parallel to the production of NADPH during linear electron flow, but this does not provide the correct ATP:NADPH ratio for CO_2 fixation (Baker et al. 2007). As a result, photoautotrophs must supply additional ATP via the photosynthetic electron transfer chain. Suggett et al. (2010) expected that the ratio of between the e^- $(O_2)^{-1}$ and e^- $(CO_2)^{-1}$ would be systematically different. The fluorescence technique measures a gross ETR that is related to gross primary production (Suggett et al. 2001). The ^{14}C technique measures a net carbon incorporation which does not account for the energy storage in terms of N and P, energy costs associated with N and P metabolic processes (e.g. nutrient uptake), or respiratory consumption (Williams & Lefevre 1996, Marra & Barber 2004, Corno et al. 2006). Despite the differences in principle, our ^{14}C estimates are close to gross primary production because incubation time was short (2 h), and P-E curves were fitted in such a way that production becomes 0 when the light intensity approaches 0. As such, our radiocarbon-based estimates approximate gross primary production rates. Therefore, we conclude that the methodological differences in the ^{14}C method do not explain the major part of the discrepancy.

Second, we should consider the impacts of errors in determining the non-fluorometric parameters in the equation for FRRF-derived primary production rates, including n_{PSII}, PQ, and $1/k$. The n_{PSII} ranges from 0.001 to 0.007 mol RCII (mol chl a)$^{-1}$ (Falkowski et al. 1986). We used the average value 0.002 for n_{PSII} (Mauzerall & Greenbaum 1989), and 1.4 for PQ, although PQ can vary from 1.1 to 1.5 mol O_2 evolved (mol C fixed)$^{-1}$ depending on the N source (Laws 1991). The quantum yield of electron transport ($1/k$) ranges from 0.18 to 0.25 (Flameling & Kromkamp 1998), and we used 0.25 mol O_2 (mol photons)$^{-1}$. The uncertainty of these parameters will produce errors in P_{FRRF}. To check how the uncertainties in these parameters influence the primary production estimation, we ran Monte Carlo simulations assuming a uniform distribution within the above ranges. We used the fluorescence parameters from a station that showed the median value in the differences between the 2 methods. We randomly selected 10 000 sets of the 3 parameters from the above ranges assuming a uniform distribution. Fig. 8 shows the density distribution of the primary production rates calculated from the set of 10 000 random parameters. From this distribution, our estimated primary production rate

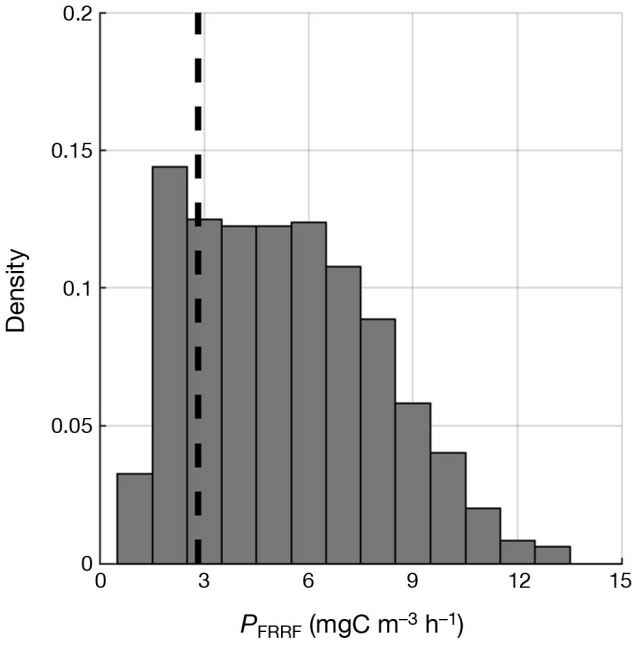

Fig. 8. Density distribution of the primary production rates calculated from 10000 Monte Carlo simulations to test whether the uncertainties of the 3 predetermined parameters (n_{PSII}, PQ, and $1/k$; fluorescence parameters defined in Table 1) can explain the overestimation of primary production. Each run used the measured FRRF variables from a station in the Yellow Sea, and 3 predetermined parameters were randomly chosen from uniform distributions of known ranges. The dashed line is the FRRF-derived primary production rate of 2.83 mg C m^{-3} h^{-1} (p = 0.28), indicating that the uncertainties of the predetermined parameters cannot explain the overestimation

(2.83 mg C m^{-3} h^{-1}) has the probability p = 0.28 (other cases result in a similar level of probability). In other words, the combination of non-fluorometric parameters we used produced a primary production estimate that occupied the lower 28% of the distribution of the 10 000 estimates by random combination. Therefore, it is not likely that we measured high primary production rates because of the non-fluorometric parameters used.

The third possibility is that the overestimation of the fluorescence technique is due to complicated pathways of electron transport. Several studies have shown that the fluorescence technique may overestimate the rates at high light levels, presumably due to the impact of physiological processes such as cyclic electron flow, the Mehler reaction, and photorespiration (Raateoja 2004, Fujiki et al. 2007, Cheah et al. 2011). Cyclic electron flows occur around PSII, with some electrons returning from the acceptor side (plastoquinol, PQH_2) of PSII to the donor side at light saturation (Falkowski et al. 1986, Prasil et al. 1996). In light-saturated conditions, the cyclic electron flow is estimated to be ~15% of the total electron transport in PSII (Falkowski et al. 1986). In the Mehler reaction, the direct reduction of O_2 to superoxide is driven by the reducing side of PS (Badger 1985, Asada 1999). O_2 reduction by the Mehler reaction accounts for approximately 50% of total electron transport and is less important under light-limited conditions (Kana 1992, Badger et al. 2000). Photorespiration is low in aquatic photoautotrophs (Falkowski & Raven 2007); therefore, the effect of photorespiration may not be substantial. These physiological processes provide electrons with an alternative electron sink which is not related to carbon assimilation (Kana 1992, Lewitus & Kana 1995). In this case, the ETR will deviate from the carbon assimilation rate. When we divided primary production rates into 2 subsets according to the light saturation intensities (Fig. 9), we found that the discrepancy between FRRF- and ^{14}C-based primary production rates was greater in the high light intensity set. The slope value increased from 1.66 (r^2 = 0.92, p < 0.001, n = 11) to 2.1 (r^2 = 0.91, p < 0.001, n = 11) above the light-saturated condition (Fig. 9). The regression coefficient was about 27% larger in

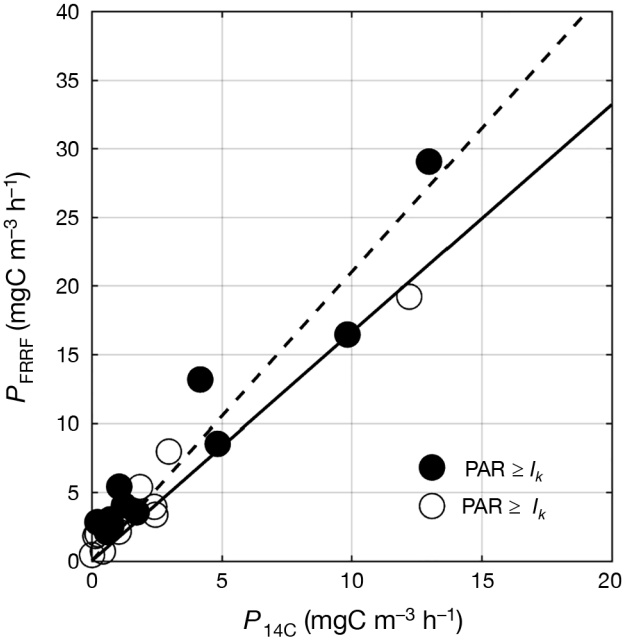

Fig. 9. Relationship between the primary production rates using FRRF-based and ^{14}C methods. The data points were grouped by the incident photosynthetically active radiation (PAR) values. Solid circles: PAR ≥ I_k (slope = 2.1, r^2 = 0.91, p < 0.001, n = 11; I_k is the light intensity at saturation). Open circles: PAR < I_k (slope = 1.66, r^2 = 0.92, p < 0.001, n = 11). The solid line and dashed line are the regression lines in PAR < I_k and PAR ≥ I_k, respectively

the high light. This supports the interpretation that FRRF-based production rates overestimate the production rates, as the proportionality of ETR to carbon assimilation rate changes as light intensity increases.

4.2. 'Bottle effects' associated with the ^{14}C technique

Above, we examined 3 possible sources of overestimation by FRRF. However, the fourth possibility is that the ^{14}C technique may underestimate the true production rate. The most probable cause of this error is associated with the so-called 'bottle effect.' The bottle effect occurs as samples are incubated within a confined volume so that the physiology and growth of algal cells are influenced by artificial factors such as trace metals, toxic contamination, constant excessive light intensity, cessation of material flow, and grazing (Jackson 1983, Gallegos & Platt 1985, Cullen et al. 1992). Since our measurements were conducted in coastal waters, we can exclude the effects of trace metals or toxic contamination of the bottles. As we have examined individual P-E curves (typically with 10–12 pseudoreplicates) for fitness, the impacts of grazing should be minimal. Another factor may be associated with photoinhibition under prolonged exposure to high light (Prasil et al. 1992, Macedo et al. 2002, From et al. 2014). Therefore, we further examined the effect of prolonged exposure to excessive light during incubations. For this goal, we conducted experiments on monocultures of 3 species. The experimental setups were the same as with ^{14}C incubations. We followed changes in the fluorometric variables during the course of 2 h incubations. Figs. 10 & 11 show the time course for fluorescence variables measured by the FIRe fluorometer during these incubations. Initial F_v/F_m values were close to the theoretical maximum (0.65). F_v/F_m values of *Skeletonema* sp. gradually decreased under all ambient light levels during the incubation (Fig. 10a). In particular, these values were different with each ambient light intensity. The rate of change in F_v/F_m under high light exposure was greater than that under low light. In *Heterocapsa circularisquama*, F_v/F_m values dropped sharply in all ambient light intensities after 5 min, and continued to decrease under high light (Fig. 10b). On the other hand, in *Coscinodiscus oculoides*, F_v/F_m values decreased only under the highest light (Fig. 10c). The functional absorption cross section (σ_{PSII}) did not change during incubations in all species (Fig. 11). However, the values of σ_{PSII} differed among species. The values of σ_{PSII} were higher in *Skeletonema* sp. than in other species, ranging from 201×10^{-20} to 228×10^{-20} m^2 photon^{-1} (Fig. 11a). σ_{PSII} values were lowest in *C. oculoides* at 83×10^{-20} to 97×10^{-20} m^2 photon^{-1} (Fig. 11c). The σ_{PSII} values were inversely related to cell size (*Skeletonema* sp.: <20 µm; *H. circularisquama*: 20–28 µm; *C. ocu-*

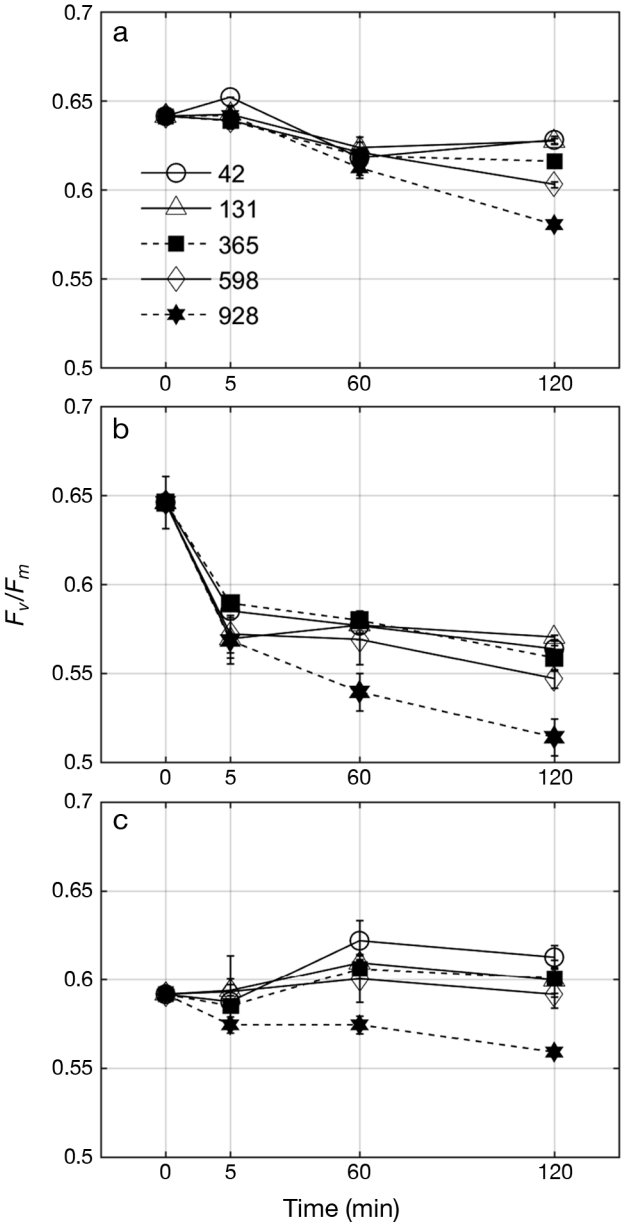

Fig. 10. Changes in the potential photochemical efficiency through time under 5 light intensities (42, 131, 365, 598, 928 µmol m^{-2} s^{-1}) during the short-term incubation of (a) *Skeletonema* sp., (b) *Heterocapsa circularisquama*, and (c) *Coscinodiscus oculoides*. Fluorescence parameters are defined in Table 1

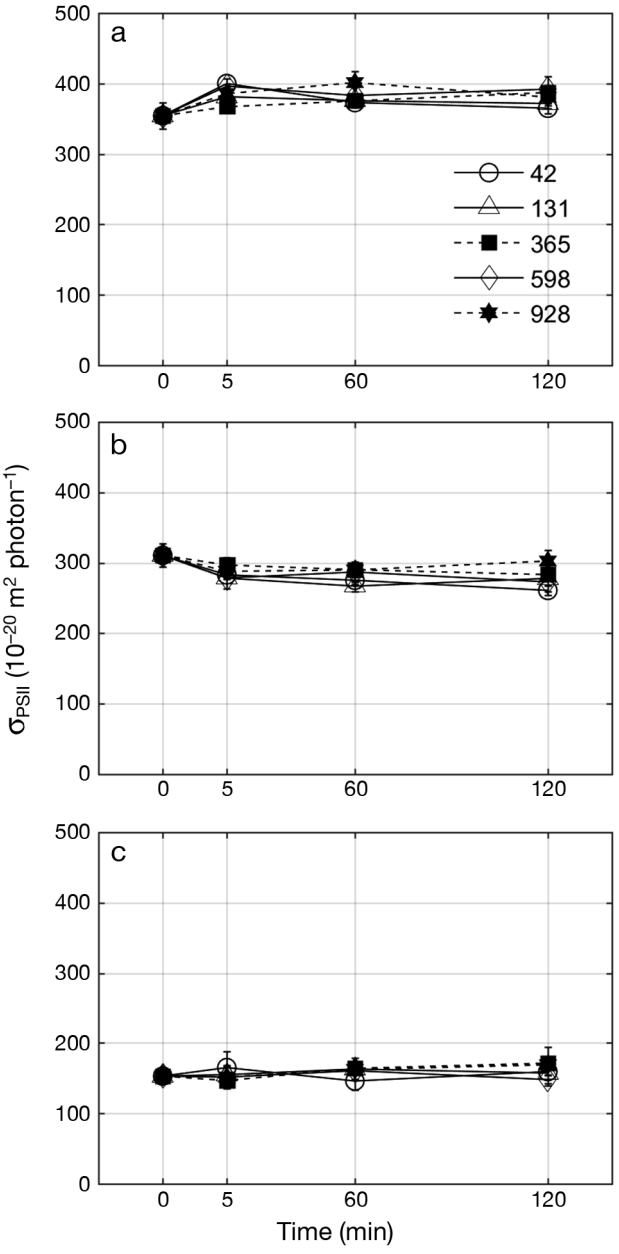

Fig. 11. Changes in the functional absorption cross section for 450 nm through time at 5 light intensities (42, 131, 365, 598, 928 µmol m^{-2} s^{-1}) during the short-term incubation of (a) *Skeletonema* sp., (b) *Heterocapsa circularisquama*, and (c) *Coscinodiscus oculoides*. Fluorescence parameters are defined in Table 1

loides: 70–90 µm), indicating package effects. Although the functional absorption cross sections did not change during the incubations, the photochemical efficiency decreased by photoinhibition. These experiments showed that production rates could decrease under prolonged exposure to high irradiance. The extent and time course of the photoinhibition differed by species. Considering only changes in the rate of photochemical efficiency in these experiments, primary production could be reduced by about 2–20% due to the bottle effects. Therefore, underestimation from bottle effects would vary depending on the composition and physiological condition of the natural communities. Considering all of these possibilities together, we conclude that the true primary production rates would be lower than the FRRF estimates but higher than the ^{14}C estimates.

4.3. Relationship between $\Phi_{e,C}$ and environmental variables

Many regional studies have shown that $\Phi_{e,C}$ in natural communities correlates with environmental factors such as macro- and micronutrients, temperature, salinity, light intensity, water transparency, and chl *a* (Lawrenz et al. 2013, Schuback et al. 2017, Morelle et al. 2018). Mostly these relationships are empirical rather than mechanistic. The *in situ* variability of $\Phi_{e,C}$ with nutrients appears to be in contrast with laboratory studies that showed that in continuous cultures $\Phi_{e,C}$ is independent of nitrogen limitation (Halsey et al. 2010, 2011, 2013). Such discrepancies between field and lab data can be attributed to unbalanced growth of natural phytoplankton and to errors in estimating gross primary production from short-term ^{14}C incubation experiments (Kolber et al. 1988, Babin et al. 1996, Lawrenz et al. 2013).

Our field data also revealed a wide range of $\Phi_{e,C}$ variation, from 5.5 to 71.3 mol e^- (mol CO_2)$^{-1}$. To better understand environmental controls of $\Phi_{e,C}$, we examined the Spearman rank correlation among all measured variables. Because the relationship among the variables in general can be best described by a power function (Fig. 12), we log-transformed variables. The sample number was reduced from 22 to 15 in this analysis because we excluded the samples with any missing terms. Regardless of whether this log-transformation was used, the Spearman correlation matrix was the same, as the Spearman correlation uses ranks. $\Phi_{e,C}$ showed a significant negative correlation with nitrate + nitrite, phosphates, K_{PAR}, and chl *a*, and a significant positive correlation with temperature (Table 5). However, the environmental variables also showed a significant correlation among themselves. Chl *a* showed a significant correlation with all variables except temperature. The positive correlation between the nutrients and chl *a* is expected and easily

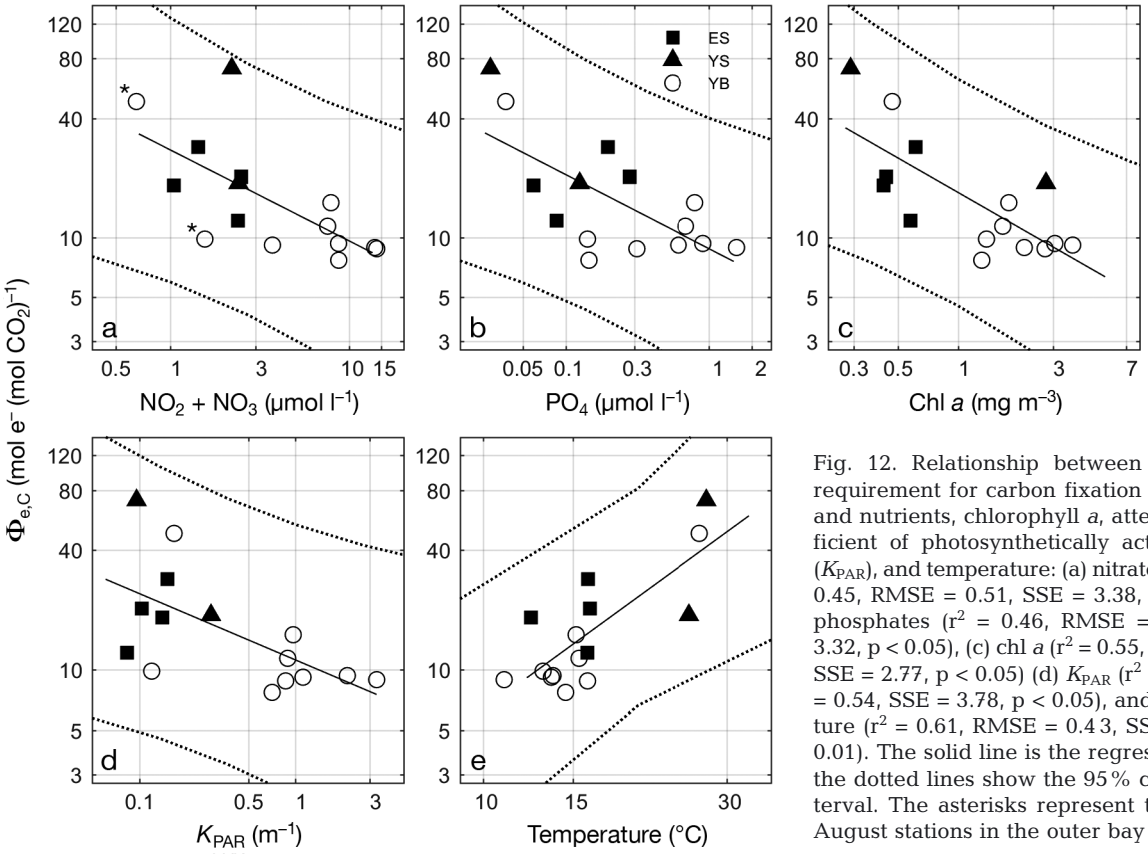

Fig. 12. Relationship between the electron requirement for carbon fixation ($\Phi_{e,C}$, mol e$^-$) and nutrients, chlorophyll *a*, attenuation coefficient of photosynthetically active radiation (K_{PAR}), and temperature: (a) nitrate + nitrite (r^2 = 0.45, RMSE = 0.51, SSE = 3.38, $p < 0.01$), (b) phosphates (r^2 = 0.46, RMSE = 0.51, SSE = 3.32, $p < 0.05$), (c) chl *a* (r^2 = 0.55, RMSE = 0.46, SSE = 2.77, $p < 0.05$) (d) K_{PAR} (r^2 = 0.39, RMSE = 0.54, SSE = 3.78, $p < 0.05$), and (e) temperature (r^2 = 0.61, RMSE = 0.4 3, SSE = 2.43, $p < 0.01$). The solid line is the regression line and the dotted lines show the 95% confidence interval. The asterisks represent the April and August stations in the outer bay of Yeosu Bay

understood. Higher K_{PAR} can result from higher river runoffs, tidal mixing, or higher chl *a*. Thus, the variables related to the above negative correlations can be interpreted as manifesting a state of nutrient limitation.

Temperature was the second most significant factor for $\Phi_{e,C}$. However, temperature did not show any significant correlation with other variables except $\Phi_{e,CC}$ and K_{PAR}. The effect of temperature on $\Phi_{e,C}$ may be indirect, as it reflects the state of stratification, which in turn modulates nutrient supply and light availability in the upper layer (Mousing et al. 2014, Hughes et al. 2018). The negative correlation of temperature with nutrients, K_{PAR}, and chl *a* supports this interpretation, although only the correlation with K_{PAR} was significant. Our surveys were conducted in 3 regional seas that lie along a gradient of optical complexity and distinctive environmental characteristics. These stations represent seasonally stratified (most stations) or tidally mixed (the inner bay of the YB). The inner bay stations were shallow (<15 m) and well mixed by tides. They were also under the influence of freshwater discharge. In Fig. 12, these stations form a cluster of high nutrients, high chl *a*, high K_{PAR}, and low temperature. The outer bay station in the YB (Fig. 1) was at the opposite extreme. Within the stream of the oligotrophic Kuroshio, it was deeper (>45 m) and underwent seasonal stratification. In April, there was no nutri-

Table 5. Spearman rank correlation matrix between abiotic and biological parameters in surface waters. $\Phi_{e,C}$: electron requirement of carbon fixation; N: nitrate + nitrite; P: phosphate; Temp: temperature; Sal: salinity; PAR: photosynthetically active radiation; K_{PAR}: vertical attenuation coefficient of PAR; chl *a*: chlorophyll *a* concentration. The asterisks indicate significance level (**p < 0.01, *p < 0.05)

	$\Phi_{e,C}$	N	P	Temp	Sal	PAR	K_{PAR}	Chl *a*
$\Phi_{e,C}$	1	−0.78**	−0.59*	0.68**	0.23	0.14	−0.60*	−0.63*
N		1	0.76**	−0.31	−0.53*	−0.38	0.68**	0.63*
P			1	−0.49	−0.32	−0.25	0.82**	0.70**
Temp				1	−0.19	−0.04	−0.47*	−0.36
Sal					1	0.54*	−0.59*	−0.60*
PAR						1	−0.41	−0.33
K_{PAR}							1	0.80**
Chl *a*								1

cline in the outer station in the YB, while in August, a nutricline accompanying a thermocline was well developed (Fig. 3). As the season progressed from spring to summer, $\Phi_{e,C}$ increased by approximately 5-fold (Fig. 6). A similar pattern was observed at the YS stations in the summer (Fig. 12). The ES stations showed an intermediate level of electron requirements. These stations were sampled in May during the later stage of spring blooms. Therefore, the whole dataset represents a gradient from a well-mixed turbid environment to clear surface water in a strongly stratified water body. Because the YB stations covered the whole range of this gradient, they contributed the largest portion of the variance of many variables.

One might ask if the stations in the other regions showed different statistical characteristics. However, there was no regional bias in the relationships between ETR^B (chlorophyll-specific ETR) and P^B (Fig. 5) or P_{FRRF} and P_{14C} (Fig. 7). For example, the slope and *y*-intercept of the regression between P_{FRRF} and P_{14C} were not much different when all the stations were considered ($y = 0.56 + 0.56x$, Fig. 7a) or when only the YB stations were counted ($y = 0.55 + 0.57x$, Fig. 7b). A similar statement can be made for the relationships between $\Phi_{e,C}$ and environmental variables (Fig. 12). The YS station in summer behaved similarly to the outer bay station in the YB in summer. Other stations in the YS and ES were located along the gradient formed by the inner and outer YB stations. This is reassuring in that the stations, as a whole, represent a wide range of environmental characteristics and sampling depths (Fig. 2). Therefore, we can take advantage of this to derive a statistical model for predicting $\Phi_{e,C}$ from environmental variables. If we fit a multiple linear regression model using only the significant variables after log-transformation, it becomes a multiplicative model.

$$\Phi_{e,C} = 0.35 \times N^{-0.30} \times P^{0.18} \times {K_{PAR}}^{0.21} \times (\text{chl } a)^{-0.58} \times \text{Temp}^{1.70} \quad (11)$$

This multiplicative model shows higher R^2 (0.93, $p < 0.01$), as compared to the additive model ($R^2 = 0.82$, $p < 0.01$).

$$\Phi_{e,C} = -0.72 \times N + 1.09 \times P + 2.66 \times \text{Temp} + 6.39 \times K_{PAR} - 7.09 \times (\text{chl } a) - 15.17 \quad (12)$$

To reduce the errors of multicollinearity, we can use fewer variables and choose the 3 variables that show highest correlation with the electron requirement:

$$\Phi_{e,C} = 0.43 \times N^{-0.08} \times (\text{chl } a)^{-0.35} \times \text{Temp}^{1.35} \quad (13)$$

The above model results in $R^2 = 0.85$ ($p < 0.01$). If we use the minimal model with only N and Temp, we obtain:

$$\Phi_{e,C} = 0.40 \times N^{-0.28} \times \text{Temp}^{1.44} \quad (14)$$

This minimal model still shows a high $R^2 = 0.74$ ($p < 0.01$).

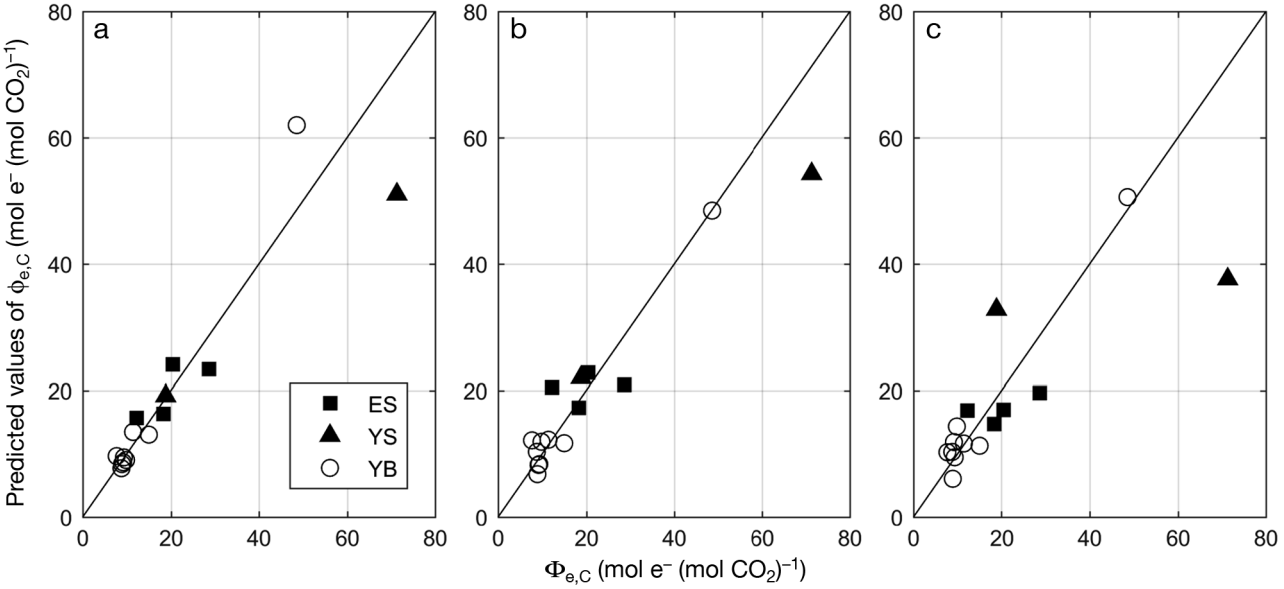

Fig. 13. Comparison of *in situ* electron requirement of carbon fixation values ($\Phi_{e,C}$, mol e$^-$) and predicted values of $\Phi_{e,C}$ by 3 proposed algorithms: (a) the full model using all significant environmental variables, i.e. nitrate + nitrite, phosphate, chlorophyll *a*, attenuation coefficient of photosynthetically active radiation (PAR), and temperature ($r = 0.93$, $p < 0.01$); (b) the partial model using 3 variables, namely nitrate + nitrite, chl *a*, and temperature ($r = 0.89$, $p < 0.01$); and (c) the minimal model using only 2 variables, nitrate + nitrite and temperature ($r = 0.86$, $p < 0.01$). The solid line indicates the 1:1 line. ES: East Sea; YS: Yellow Sea; YB: Yeosu Bay

We further compared the electron requirements predicted by the 3 algorithms with the actual values (Fig. 13). The predicted values show a good correspondence with the actual values. Even the minimal model shows a fairly high level of correspondence (r = 0.86). There seems to be no significant bias between the regional seas, which is consistent with the observation above that there seems to be no significant regional bias in the relationship among the variables.

To summarize, our data revealed that nutrient supply and the state of stratification are the major determinants of the electron requirement for carbon fixation in this region. However, our data have a limited number of observations (n = 15), and not all seasons were covered in the YS and ES. Therefore, further investigations are needed to test how these algorithms will hold for other areas and other seasons.

Acknowledgements. We thank Soonmi Lee, Joo-eun Yoon, and Su In Kim for collaborating in the field and Kevin Wyman for discussion. This research was supported by the 'Technology development for Practical Applications of Multi-Satellite data to maritime issues' funded by the Ministry of Ocean and Fisheries, Korea. M.Y.G. was partly supported by the NASA Ocean Biology and Biogeochemistry Program.

LITERATURE CITED

Aiken J, Rees N, Hooker S, Holligan P and others (2000) The Atlantic Meridional Transect: overview and synthesis of data. Prog Oceanogr 45:257–312

Asada K (1999) The water-water cycle on chloroplasts: scavenging of active oxygens and dissipation of excess photons. Annu Rev Plant Physiol Plant Mol Biol 50:601–639

Babin M, Morel A, Claustre H, Bricaud A, Kolber Z, Falkowski PG (1996) Nitrogen- and irradiance-dependent variations of the maximum quantum yield of carbon fixation in eutrophic, mesotrophic and oligotrophic marine systems. Deep Sea Res I 43:1241–1272

Badger MR (1985) Photosynthetic oxygen exchange. Annu Rev Plant Physiol 36:27–53

Badger MR, von Caemmerer S, Ruuska S, Nakano H (2000) Electron flow to oxygen in higher plants and algae: rates and control of direct photoreduction (Mehler reaction) and rubisco oxygenase. Philos Trans R Soc B 355: 1433–1446

Baker NR, Oxborough K, Lawson T, Morison JIL (2001) High resolution imaging of photosynthetic activities of tissues, cells and chloroplasts in leaves. J Exp Bot 52:615–621

Baker NR, Harbinson J, Kramer DM (2007) Determining the limitations and regulation of photosynthetic energy transduction in leaves. Plant Cell Environ 30: 1107–1125

Behrenfeld MJ, Randerson JT, McClain CR, Feldman GC and others (2001) Biospheric primary production during an ENSO transition. Science 291:2594–2597

Boyd PW, Aiken J, Kolber Z (1997) Comparison of radiocarbon and fluorescence based (pump and probe) measurements of phytoplankton photosynthetic characteristics in the Northeast Atlantic Ocean. Mar Ecol Prog Ser 149: 215–226

Cheah W, McMinn A, Griffiths FB, Westwood KJ and others (2011) Assessing Sub-Antarctic Zone primary productivity from fast repetition rate fluorometry. Deep Sea Res II 58:2179–2188

Corno G, Letelier RM, Abbott MR, Karl DM (2006) Assessing primary production variability in the North Pacific subtropical gyre: a comparison of fast repetition rate fluorometry and ^{14}C measurements. J Phycol 42:51–60

Cullen JJ, Lewis MR, Davis CO, Barber RT (1992) Photosynthetic characteristics and estimated growth-rates indicate grazing is the proximate control of primary production in the Equatorial Pacific. J Geophys Res Oceans 97: 639–654

Estevez-Blanco P, Cermeno P, Espineira M, Fernandez E (2006) Phytoplankton photosynthetic efficiency and primary production rates estimated from fast repetition rate fluorometry at coastal embayments affected by upwelling (Rias Baixas, NW of Spain). J Plankton Res 28: 1153–1165

Falkowski PG (1994) The role of phytoplankton photosynthesis in global biogeochemical cycles. Photosynth Res 39:235–258

Falkowski PG, Raven JA (2007) Aquatic photosynthesis. Princeton University Press, Princeton, NJ

Falkowski PG, Fujita Y, Ley A, Mauzerall D (1986) Evidence for cyclic electron flow around photosystem-II in *Chlorella pyrenoidosa*. Plant Physiol 81:310–312

Field CB, Behrenfeld MJ, Randerson JT, Falkowski P (1998) Primary production of the biosphere: integrating terrestrial and oceanic components. Science 281: 237–240

Flameling IA, Kromkamp J (1998) Light dependence of quantum yields for PSII charge separation and oxygen evolution in eucaryotic algae. Limnol Oceanogr 43: 284–297

From N, Richardson K, Mousing EA, Jensen PE (2014) Removing the light history signal from normalized variable fluorescence (F_v/F_m) measurements on marine phytoplankton. Limnol Oceanogr Methods 12:776–783

Fujiki T, Suzue T, Kimoto H, Saino T (2007) Photosynthetic electron transport in *Dunaliella tertiolecta* (Chlorophyceae) measured by fast repetition rate fluorometry: relation to carbon assimilation. J Plankton Res 29: 199–208

Gallegos CL, Platt T (1985) Vertical advection of phytoplankton and productivity estimates: a dimensional analysis. Mar Ecol Prog Ser 26:125–134

Gorbunov MY, Falkowski PG, Kolber ZS (2000) Measurement of photosynthetic parameters in benthic organisms in situ using a SCUBA-based fast repetition rate fluorometer. Limnol Oceanogr 45:242–245

Gorbunov MY, Kolber ZS, Lesser MP, Falkowski PG (2001) Photosynthesis and photoprotection in symbiotic corals. Limnol Oceanogr 46:75–85

Guillard RRL (1975) Culture of phytoplankton for feeding marine invertebrates. In: Smith WL, Chanley MH (eds) Culture of marine invertebrate animals. Plenum Press, New York, NY, p 26–60

Halsey KH, Milligan AJ, Behrenfeld MJ (2010) Physiological optimization underlies growth rate-independent chloro-

phyll-specific gross and net primary production. Photosynth Res 103:125–137
Halsey KH, Milligan AJ, Behrenfeld MJ (2011) Linking time-dependent carbon fixation efficiencies in *Dunaliella tertiolecta* (Chlorophyceae) to underlying metabolic pathways. J Phycol 47:66–76
Halsey KH, O'Malley RT, Graff JR, Milligan AJ, Behrenfeld MJ (2013) A common partitioning strategy for photosynthetic products in evolutionarily distinct phytoplankton species. New Phytol 198:1030–1038
Holmes RW (1970) The Secchi disk in turbid coastal waters. Limnol Oceanogr 15:688–694
Hughes DJ, Varkey D, Doblin MA, Ingleton T and others (2018) Impact of nitrogen availability upon the electron requirement for carbon fixation in Australian coastal phytoplankton communities. Limnol Oceanogr 63: 1891–1910
Jackson GA (1983) Zooplankton grazing effects on ^{14}C-based phytoplankton production measurements: a theoretical study. J Plankton Res 5:83–94
Kana TM (1992) Relationship between photosynthetic oxygen cycling and carbon assimilation in *Synechococcus* Wh7803 (Cyanophyta). J Phycol 28:304–308
Kirk J (1977) Use of a quanta meter to measure attenuation and underwater reflectance of photosynthetically active radiation in some inland and coastal south-eastern Australian waters. Mar Freshw Res 28:9–21
Kolber Z, Falkowski PG (1993) Use of active fluorescence to estimate phytoplankton photosynthesis in situ. Limnol Oceanogr 38:1646–1665
Kolber Z, Zehr J, Falkowski P (1988) Effects of growth irradiance and nitrogen limitation on photosynthetic energy conversion in photosystem II. Plant Physiol 88:923–929
Kolber ZS, Prasil O, Falkowski PG (1998) Measurements of variable chlorophyll fluorescence using fast repetition rate techniques: defining methodology and experimental protocols. Biochim Biophys Acta Bioenerg 1367:88–106
Kromkamp JC, Forster RM (2003) The use of variable fluorescence measurements in aquatic ecosystems: differences between multiple and single turnover measuring protocols and suggested terminology. Eur J Phycol 38: 103–112
Lawrenz E, Silsbe G, Capuzzo E, Ylöstalo P and others (2013) Predicting the electron requirement for carbon fixation in seas and oceans. PLOS ONE 8(3):e58137
Laws EA (1991) Photosynthetic quotients, new production and net community production in the open ocean. Deep Sea Res A Oceanogr Res Pap 38:143–167
Lewitus AJ, Kana TM (1995) Light respiration in six estuarine phytoplankton species: contrasts under photoautotrophic and mixotrophic growth conditions. J Phycol 31: 754–761
Longhurst A, Sathyendranath S, Platt T, Caverhill C (1995) An estimate of global primary production in the ocean from satellite radiometer data. J Plankton Res 17: 1245–1271
Macedo MF, Duarte P, Ferreira JG (2002) The influence of incubation periods on photosynthesis-irradiance curves. J Exp Mar Biol Ecol 274:101–120
Marra J, Barber RT (2004) Phytoplankton and heterotrophic respiration in the surface layer of the ocean. Geophys Res Lett 31:L09314
Mauzerall D, Greenbaum NL (1989) The absolute size of a photosynthetic unit. Biochim Biophys Acta 974:119–140
Melrose DC, Oviatt CA, O'Reilly JE, Berman MS (2006) Comparisons of fast repetition rate fluorescence estimated primary production and ^{14}C uptake by phytoplankton. Mar Ecol Prog Ser 311:37–46
Milligan AJ, Halsey KH, Behrenfeld MJ (2015) Advancing interpretations of ^{14}C-uptake measurements in the context of phytoplankton physiology and ecology. J Plankton Res 37:692–698
Moore CM, Suggett D, Holligan PM, Sharples J and others (2003) Physical controls on phytoplankton physiology and production at a shelf sea front: a fast repetition-rate fluorometer based field study. Mar Ecol Prog Ser 259: 29–45
Moore CM, Suggett DJ, Hickman AE, Kim YN and others (2006) Phytoplankton photoacclimation and photoadaptation in response to environmental gradients in a shelf sea. Limnol Oceanogr 51:936–949
Morel A, Prieur L (1977) Analysis of variations in ocean color. Limnol Oceanogr 22:709–722
Morelle J, Schapira M, Orvain F, Riou P and others (2018) Annual phytoplankton primary production estimation in a temperate estuary by coupling PAM and carbon incorporation methods. Estuaries Coasts 41:1337–1355
Mousing EA, Ellegaard M, Richardson K (2014) Global patterns in phytoplankton community size structure—evidence for a direct temperature effect. Mar Ecol Prog Ser 497:25–38
Oxborough K, Baker N (1997) Resolving chlorophyll *a* fluorescence images of photosynthetic efficiency into photochemical and non-photochemical components—calculation of *qP* and *Fv*′/*Fm*′ without measuring F_0′. Photosynth Res 54:135–142
Platt T, Gallegos CL, Harrison WG (1980) Photoinhibition of photosynthesis in natural assemblages of marine phytoplankton. J Mar Res 38:687–701
Prasil O, Adir N, Ohad I (1992) Dynamics of photosystem II: mechanism of photoinhibition and recovery process. Top Photosynth 11:295–348
Prasil O, Kolber Z, Berry JA, Falkowski PG (1996) Cyclic electron flow around photosystem II *in vivo*. Photosynth Res 48:395–410
Raateoja MP (2004) Fast repetition rate fluorometry (FRRF) measuring phytoplankton productivity: a case study at the entrance to the Gulf of Finland, Baltic Sea. Boreal Environ Res 9:263–276
Raateoja M, Seppälä J, Kuosa H (2004) Bio-optical modelling of primary production in the SW Finnish coastal zone, Baltic Sea: fast repetition rate fluorometry in Case 2 waters. Mar Ecol Prog Ser 267:9–26
Schuback N, Hoppe CJ, Tremblay JÉ, Maldonado MT, Tortell PD (2017) Primary productivity and the coupling of photosynthetic electron transport and carbon fixation in the Arctic Ocean. Limnol Oceanogr 62:898–921
Smyth TJ, Pemberton KL, Aiken J, Geider RJ (2004) A methodology to determine primary production and phytoplankton photosynthetic parameters from fast repetition rate fluorometry. J Plankton Res 26:1337–1350
Suggett D, Kraay G, Holligan P, Davey M, Aiken J, Geider R (2001) Assessment of photosynthesis in a spring cyanobacterial bloom by use of a fast repetition rate fluorometer. Limnol Oceanogr 46:802–810
Suggett DJ, Oxborough K, Baker NR, MacIntyre HL, Kana TM, Geider RJ (2003) Fast repetition rate and pulse amplitude modulation chlorophyll *a* fluorescence measurements for assessment of photosynthetic electron

transport in marine phytoplankton. Eur J Phycol 38: 371–384

Suggett DJ, Moore CM, Maranon E, Omachi C, Varela RA, Aiken J, Holligan PM (2006) Photosynthetic electron turnover in the tropical and subtropical Atlantic Ocean. Deep Sea Res II 53:1573–1592

Suggett DJ, Prášil O, Borowitzka MA (2010) Chlorophyll *a* fluorescence in aquatic sciences: methods and applications. Springer, London

Williams PJL, Lefevre D (1996) Algal ^{14}C and total carbon metabolisms. 1. Models to account for the physiological processes of respiration and recycling. J Plankton Res 18: 1941–1959

Yoon JE, Park J, Yoo S (2012) Comparison of primary productivity algorithms for Korean waters. Ocean Sci J 47: 473–487

Editorial responsibility: Nicholas Tolimieri, Seattle, Washington, USA

Submitted: November 28, 2018; Accepted: July 22, 2019
Proofs received from author(s): September 19, 2019